Chemical Engineering Journal 446 (2022) 137000

Contents lists available at ScienceDirect

Chemical Engineering Journal

journal homepage: www.elsevier.com/locate/cej

Surface plasma resonance biosensing of phosphorylated proteins via pH-adjusted specific binding of phosphate residues with UiO-66

Nini Luo [a,b,1], Yue Shu [b,1], Chuanlong Zhu [a], Xiaoxue Cheng [b], Lixue Chen [c], Jiang Wang [c], Rui Liu [a], Huangxian Ju [d], Wei Cheng [b,*], Qianfeng Xia [a,*]

[a] Key Laboratory of Tropical Translational Medicine of Ministry of Education, NHC Key Laboratory of Tropical Disease Control, School of Tropical Medicine and The Second Affiliated Hospital, Hainan Medical University, Haikou, Hainan 571199, PR China
[b] The Center for Clinical Molecular Medical Detection, The First Affiliated Hospital of Chongqing Medical University, Chongqing 400016, PR China
[c] Laboratory Research Center, The First Affiliated Hospital of Chongqing Medical University, Chongqing 400016, PR China
[d] State Key Laboratory of Analytical Chemistry for Life Science, School of Chemistry and Chemical Engineering, Nanjing University, Nanjing 210023, PR China

ARTICLE INFO

Keywords:
Surface plasma resonance
Metal-organic framework
UiO-66
Biosensor
Protein phosphorylation

ABSTRACT

The abnormal protein phosphorylation is closely related to a series of diseases including cancers, neurodegeneration, and other immune/inflammatory disorders. However, a simple, accurate, and pragmatic methodology for the direct detection of phosphorylation levels of target proteins is largely unavailable. Herein, a surface plasma resonance (SPR) biosensor was developed to detect phosphorylated protein based on significant SPR enhancement using UiO-66 and its high affinity for phosphate residues. Furthermore, the pH of the incubation buffer and the NaOH concentration in the washing solution to eliminate nonspecific adsorption of nanoparticles on the chip surface were optimized to adjust the surface charges of UiO-66. This improved the specificity and sensitivity of the proposed method. The designed biosensor could distinguish 1% phosphorylated peptides from non-phosphorylated peptides background. Moreover, the method could directly analyze the phosphorylation level of target protein in complex samples such as cell or tissue extracts without requiring a purification step in a single workflow. This simple and robust biosensor is a sensitive, accurate, and pragmatic toolbox to detect phosphorylated proteins without destroying the protein structure and can significantly facilitate phosphoproteomics and clinical diagnosis research.

1. Introduction

Protein phosphorylation, a process involving the attachment of phosphate groups to specific amino acid residues (serine (S), threonine (T), or tyrosine (Y)) in target proteins, is closely linked to various biological processes including signal transduction, apoptosis, and gene expression [1]. In the past years, it has been shown that the aberrant protein phosphorylation could lead to various diseases such as cancer, diabetes mellitus, neurodegeneration, and other immune-inflammatory disorders [2,3]. Therefore, analysis of the phosphorylated proteins is necessary for deciphering the fundamental biological processes and indicating pathogenesis and diseases development at the molecular level.

Western blotting (WB) is a commonly used technique to examine phosphorylated proteins [4,5]. However, this method requires a complex operation that can be influenced by many factors, such as the incubation temperature and time, quality of primary antibodies, cleaning solution composition, etc. that may cause poor repeatability and quantification. Advanced development in the field of mass spectrometry (MS) technology has made it possible for the sensitive, accurate, and high-throughput analysis of protein phosphorylation by detecting the mass-to-charge ratio of proteins or peptides [6,7]. Nevertheless, it requires sophisticated and expensive equipment. Also, the pretreatment of the sample may destroy the original structure of the candidate phosphoprotein.

Recently, metal oxide affinity chromatography (MOAC) has been reported to isolate the phosphorylated peptides based on Lewis acid-base-interaction between the metal oxide and phosphate group of phosphorylated peptides in an acidic environment [8–10]. Besides, several studies explored the individual metal oxides such as Zr^{4+}, Ti^{4+},

* Corresponding authors.
E-mail addresses: chengwei@hospital.cqmu.edu.cn (W. Cheng), xiaqianfeng@hainmc.edu.cn (Q. Xia).
[1] These author contributed equally to this work.

https://doi.org/10.1016/j.cej.2022.137000
Received 10 December 2021; Received in revised form 15 April 2022; Accepted 12 May 2022
Available online 14 May 2022

Fe $^{3+}$ and Zn $^{2+}$, except Si^{4+} [11,12], for their high affinity towards phosphate group and application in the field of phosphor-proteomics [13–16]. For instance, Gaurav et al. used Zn $^{2+}$-Phos-Tag SDS-PAGE to detect the phosphorylated protein at neutral pH based on Zn $^{2+}$ coordination with the protein phosphate group [17,18].

In addition, the metal–organic framework (MOF) having excellent characteristics like higher surface area, specific symmetry, and ease of modification has rapidly emerged as an alternative approach for its diverse applications [19–21]. For instance, Fe-MOF and Zr-MOF [22,23] are commonly used for the isolation and enrichment of phosphorylation peptides or proteins by forming coordination covalent bonds with phosphoric acid groups. Also, these have higher phosphate adsorption capacity than amorphous zirconium oxide nanoparticles [24]. Zhao et al. used the hydrophilic core–shell-shell structured magnetic MOF to analyze the phosphate protein. In this work, the phosphorylated proteins were hydrolyzed into separate peptide chains for further enrichment and detection by MS [25]. Similarly, Yao Wu and co-workers synthesized a new type of magnetic guanylyl-functionalized MOF nanospheres to achieve the enrichment and detection of phosphor-peptides [26]. Although these detection methods focused on the isolation and enrichment effect of MOF, the process is time-consuming requiring tedious steps like isolation, purification, and detection, and could not realize quantitative detection of phosphorylated proteins. Overall, a simple, accurate and pragmatic methodology for the direct detection of phosphorylated proteins remains an urgent requirement.

Surface plasma resonance (SPR) biosensor is a kind of optical technique that enables real-time and multiplexed detection of biomolecules using the captured probes modified on an SPR chip. The amount of the substance could be tested based on the change in refractive index in the vicinity of thin metal layers [27–32]. It is a high sensitivity, label-free, real-time, in-situ, and multiplex biomarker detection method, which has made SPR biosensors a powerful tool in many scientific fields, such as antigen–antibody interaction monitoring, immunological identification, medical diagnostics, and so on [33–35].

Recent studies found that the inherent Zr–O clusters in the UiO series of MOFs present a high affinity toward phosphoric groups and could help in realizing the remarkably enhanced uptake of phosphor-bearing phosphates or phosphonates via the formation of Zr–O–P bonds [36,37]. Inspired by this, we logically speculated that the Zr–O clusters in Zr-based MOFs could also serve as effective anchorages for the binding with phosphoric groups containing phosphorylated peptides. Numerous nanomaterials (such as gold, silver, magnetic nanomaterials, etc.) have been used to improve the SPR signals sensitivity [38,39]. For now, not many researchers use individual Zr-MOFs to enhance the SPR effect. Herein, a pH-adjusted SPR biosensor was designed for the detection of phosphorylated proteins based on the specific binding between Zr-MOF (UiO-66) and phosphate residues. In this method, UiO-66 served as a dual-functional element that not only specifically bound to phosphoprotein but also enhanced the SPR signal. Furthermore, the effect of the pH environment on the specificity combination of UiO-66 for the phosphate group was systematically investigated. This method realizes direct detection of phosphorylated residues in protein extracts without additional isolation and purification. This simple, specific, and sensitive biosensor can be an alternative platform for the direct analysis of phosphorylated proteins and peptides.

2. Materials and methods

2.1. Materials and reagents

Tris, zirconyl chloride ($ZrOCl_2{\cdot}8H_2O$), 1,4-benzenedicarboxylic acid (H_2-BDC), and N,N-Dimethy-Formamide (DMF) were purchased from Aladdin Chemistry Co., Ltd (Shanghai, China). MDA-MB-231 cells were cultured in Dulbecco's modified Eagle's medium (DMEM, HyClone; Thermo Scientific) with 10% fetal bovine serum (FBS), 100 U/mL penicillin, and 100 μg/ml streptomycin at 37 ℃ and 5% CO_2. Bovine serum albumin (BSA) was obtained from Thermo Fisher Scientific (Wilmington, USA). All cell lines were purchased from American Type Culture Collection (ATCC). Phosphorylated (PP; KpYRKNLDFEQLKC) and non-phosphorylated (NPP; KYRKNLDFEQLKC) peptides were purchased from Sangon Biotech. Co. Ltd. (Shanghai, China). Akt, Anti-total Akt antibody, Anti-p-akt antibody, and 2-(4-morpholinyl)-8-phenylchromone (LY294002) (PI3K inhibitor) were supplied by Abcam (MA, USA). HRP rabbit IgG was purchased from Beyotime (Jiangsu, China). All other reagents were of analytical grade and used without further purification. Ultrapure water, used for preparing all aqueous solutions, was from Milli-Q gradient ultrapure water system (Millipore, MA).

2.2. Apparatus

The SPR platform and sensor chips with gold array were home-built. This platform has two separate channels, each with 50 μL volume, for temporally detecting proteins. A 46 nm thick gold layer was deposited on each layer via e-beam evaporation after a 2 nm thick layer of chromium was fabricated on the SPR chip as an adhesion layer. Emitting diode (LED, 650 nm) was used as an optical source to stimulate the Surface Plasmon Resonance on the SPR chip and a polarizer was used to ensure p-polarized light for SPR measurement. The matching liquid ($n = 1.616$) was mediated between the sensor chip and prism (heavy flint glass) to avoid any air influence. All sensorgrams were evaluated by a lab-developed program written in LabVIEW. The surface morphology of the sample was examined by Scanning Electron Microscopy (SEM) (Hitachi, Japan). X-ray diffraction (XRD) patterns were obtained using a D8 focus diffractometer (Bruker AXS, Germany). The SDS-PAGE and image analysis were performed with an electrophoresis analyzer and a ChemDoc XRS system (Bio-Rad, USA), respectively.

2.3. Synthesis of UiO-66

UiO-66 samples with different sizes were synthesized according to the previously reported solvothermal route with slight modification of acetic acid (Ac) ratio and reaction time [40]. Briefly, 21 mg of $ZrOCl_2{\cdot}8H_2O$ and 50 mg of H_2-BDC were added to 6 mL of DMF with magnetic stirring until the powder fully dissolved. Subsequently, 1.5 mL of Ac was added as a modulator to adjust the size of the crystals. The resulting suspension was put into a Teflon-lined autoclave (50 mL), sealed, and heated at 120 ℃ for 24 h. Next. The suspension was cooled down to room temperature and the resultant precipitate was washed with DMF several times followed by three times washing with ethyl alcohol to remove the trapped DMF molecules. Lastly, the obtained product was overnight vacuum dried at 60 ℃ for further use.

2.4. Cell culture

Human breast cancer cell line MDA-MB-231 was obtained from the Cell Bank of the Chinese Academy of Sciences (Shanghai, China). All cells were grown in DMEM (Gibco, Gaithersburg, MD, USA) supplemented with 10% heat-inactivated FBS (Biowest, Ru du Vieux Bourg, France), 100 U/mL penicillin, and 100 mg/mL streptomycin (Beyotime Biotechnology, Shanghai, China) at 37 ℃ and 5% CO_2 (Thermo, Waltham, MA, USA). The cells were cultured as described previously [41]. In brief, the cells were subcultured for 12 h and then added with 20 μM LY294002 dissolved in RPMI 1640 with shaking for 24 h. The control group was added with the same amount of DMSO, while the other treatments were the same as the inhibitor groups. The construction of the chronic migraine (CM) rat model is described in the supplementary materials.

2.5. Western blotting

Fresh trigeminal nucleus caudalis (TNC) tissue from rats or MDA-MB-231 cells were homogenized in RIPA lysis buffer (150 mM NaCl, 0.5%

Triton X100, 50 mM Tris-HCl (pH 7.4), 25 mM NaF, 20 mM EDTA, 1 mM dithiothreitol (DTT), and 1 mM Na_3VO_4; Beyotime, China) supplemented with phenylmethylsulphonyl fluoride (PMSF, Beyotime, China), 1% protease inhibitor, and 3% phosphatase inhibitor cocktails at 4 ℃ for 1 h. The homogenate was centrifuged at 12,000 rpm at 4 ℃ for 15 min and the collected supernatants were estimated for protein concentration using a BCA Protein Assay Kit (Beyotime, China). After denaturation in Laemmli buffer (60 mM Tris-Cl (pH 6.8), 2% sodium dodecyl sulfate (SDS), 10% glycerol, 5% β-mercaptoethanol, and 0.01% bromophenol blue), equal amounts of protein (30 μg) from whole cellular homogenates were subjected to SDS-PAGE.

The proteins were transferred to a membrane, which was blocked with 5% nonfat milk at 37 ℃ for 2 h and then overnight incubated with primary antibodies at 4 ℃, including anti-NR2B (1:1000, Proteintech), anti-p-NR2B (1:500, Abcam), anti-p-Akt (1:5000, Abcam), anti-total Akt (1:5000, Abcam), anti-GADPH (1:8000, Abcam), and anti-β-actin (1:5000, Proteintech, USA), respectively. The membrane was washed with 1 × TBST buffer three times and then incubated with the horseradish peroxidase-conjugated secondary antibody (1:5000, Zhongshan Golden Bridge Bio, China) at 37 ℃ for 2 h. The membrane was washed again thrice with 1 × TBST buffer and the protein bands were illuminated with the enhanced chime-luminescence (ECL) detection kit (Millipore, USA). β-actin and GADPH were used as a loading control to normalize the protein levels.

2.6. Fabrication of antibodies microarray chip

The antibodies were immobilized on the SPR chip as described previously [9,42]. Firstly, the gold chip surface was cleaned with fresh piranha solution (70% H_2SO_4, 30% H_2O_2) for 10 min to eliminate the adsorbed organic impurities, and then rinsed thoroughly with ultrapure water. The washed gold chip was dried under nitrogen. Anti-Akt, anti-p-Akt, or anti-p-NR2B Antibodies were diluted to a final concentration of 0.5 mg/mL with GTA reaction solution and printed in replicate on the bare gold-coated (thickness 50 nm) chip. The chip was incubated at 4 °C and 80% humidity overnight before rinsing with GTA reaction solution for 30 min and deionized water for 10 min. Next, the chip was blocked with 2% (w/v) BSA in GTA reaction solution for 2 h and washed with GTA reaction solution for 30 min and deionized water for 10 min, and then dried under a stream of nitrogen before further use.

2.7. Selective detection of phosphoprotein with UiO-66 on SPR platform

The dried chip was docked into the Biacore X™ instrument socket. The running solution pH was 4.0. For each SPR measurement, GTA was initially injected into both channels of the flow chamber at a constant rate of 50 μL/min at 25 °C to establish a steady-state sensorgram. Next, 80 μL of 0.4 mg/ml total protein extract was injected into the flow chamber for 2 min and 40 s and then the injector was stopped; the injector was stopped for 1 h to form antibodies-antigen hybrid on the chip surface. Subsequently, the unbound protein was washed with the GTA reaction solution until the signal stabilized (~10 min). Next, 0.5 mg/ml of MOF was passed into the reaction system for 90 min to generate the corresponding SPR signal indicating binding with the phosphate group of phosphoproteins. Lastly, NaOH was passed into the flow chamber to remove non-specifically adsorbed UiO-66. All experiments were performed with three replicates and the average value was calculated.

3. Results and discussion

3.1. Detection principle

UiO-66 was obtained based on previously reported research (Scheme 1A) [40]. Briefly, $ZrOCl_2{\cdot}8H_2O$ and H_2-BDC were used as raw materials to synthesize UiO-66, and Ac was used to adjust its particle size. The basic principle of the SPR biosensor for the detection of phosphorylated proteins due to specific binding of phosphate residues with UiO-66 is depicted in Scheme 1B. The monoclonal antibodies were immobilized on the surface of gold chips to separate certain proteins from the protein extracts. Subsequently, UiO-66 was utilized to distinguish phosphorylated protein through Zr-O-P bond to obtain a

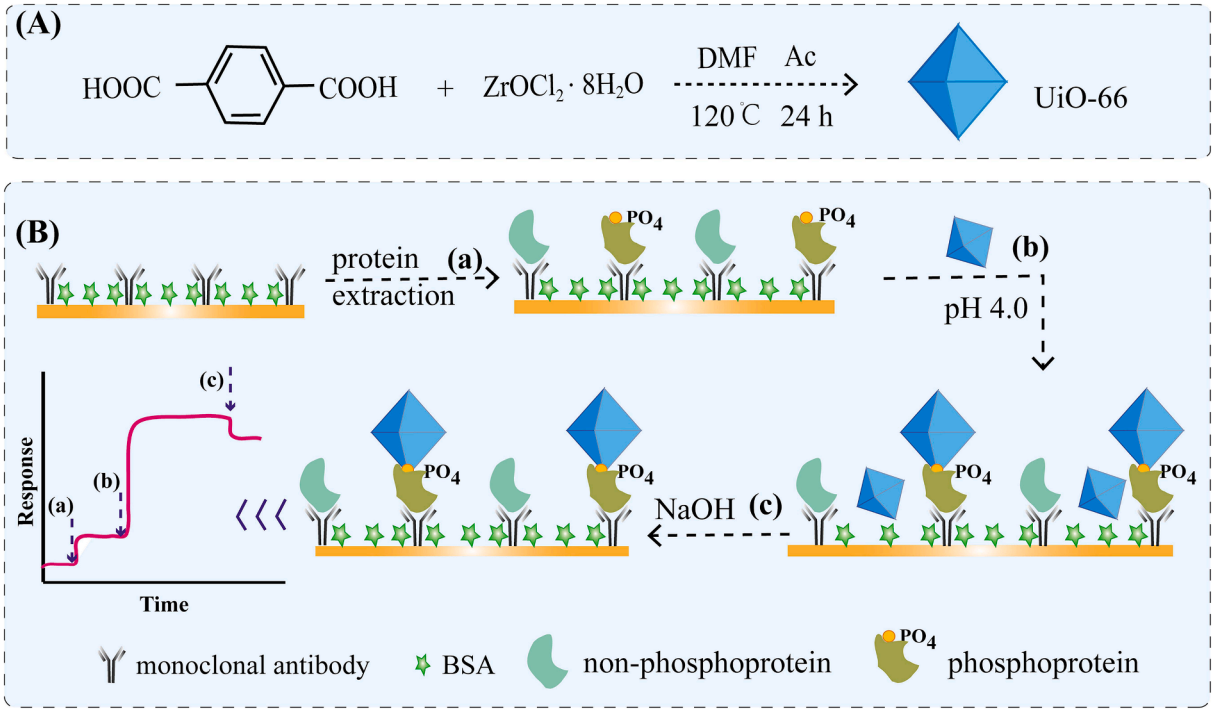

Scheme 1. Schematic illustration of (A) UiO-66 synthesis; (B) UiO-66-based SPR biosensor for the detection of phosphorylated protein. (a) The protein extract was injected into the flow chamber and then (b) UiO-66 was added. (c) NaOH solution was used to remove the non-specifically adsorbed UiO-66.

significantly enhanced SPR signal in acidic conditions. Next, the non-specific adsorption of UiO-66 was eliminated by washing with NaOH solution to improve the specificity of the designed biosensor. This method realizes the separation and detection of phosphorylated proteins on a single SPR chip interface without destroying the original structure of the protein.

3.2. Morphology and structural characterization of UiO-66

SEM was used to characterize the size and morphology of the synthetic UiO-66 (Fig. 1A and 1B). The UiO-66 particles presented good dispersion status and regular octahedral morphology with a uniform particle size of 120 ± 30 nm. Zr-based MOFs with this size range have shown high affinity toward phosphoric groups bearing phosphorylated peptides [16,24]. Also, the corresponding energy dispersive spectroscopy (EDS) element mappings of UiO-66 revealed uniform distribution of zirconium, carbon, and oxygen throughout the octahedral crystals (Fig. 1C). Furthermore, XRD was employed to characterize the crystallinity of the synthesized UiO-66 materials. Fig. 1D shows the peaks corresponding to UiO-66 particles at $2\theta = 7.64^{\circ}$ (111), 8.78° (200), 15.04° (222), 17.32° (400), which are consistent with previous studies [24,43,44]. Besides, the sharp diffraction lines in Fig. 1D suggest the high crystallinity of the UiO-66 material. All these results suggest that UiO-66 samples were fabricated successfully.

3.3. Feasibility of the biosensor strategy

Oligonucleotides chains were utilized to verify the UiO-66 binding with phosphate groups. Fig. S1 shows that the terminal phosphate modified DNA strand generated a higher SPR signal compared with that without it. This suggested that UiO-66 binding for terminal phosphate was much higher than that to an intermediate phosphate [45]. Also, it indicated that the 3′-5′ phosphodiester bond of the DNA strand could serve as a combination site for UiO-66 generating an SPR signal that remained unaffected from NaOH washing.

To further investigate the feasibility of SPR signal enhancement by UiO-66 for phosphorylation analysis, PP with phosphorylated tyrosine residue at the N'-end was modified on the surface of gold chips by using cysteine residues at the C'-ends (Fig. 2A). NPP-modified chip without phosphate groups was used as a negative control. Electrochemical impedance spectroscopy (EIS) was used to confirm the layer-by-layer modification on the gold chips using the electroactive probes $[Fe(CN)_6]^{4-/3-}$. As shown in Fig. 2B, after immobilization of peptides, the electron-transfer resistance (Ret) of the electrode increased gradually (curves b and c) compared with the bare electrode (curve a) due to the electron inert effect of peptides. A higher negative charge of PP in the acidic condition increased the EIS of the electrode (curve c) compared with NPP (curve b). Also, a significant increase in Ret (curve e) was observed for the PP-modified electrode than the NPP-modified electrode (curve d) as UiO-66 binding obstructed electron transfer to the PP-modified electrode interface. Notably, the designed peptide chain had amine, phenol (tyrosine) amide, and COOH groups in K, Y, R, and N residues, respectively. These did not produce any SPR signal in the control group compared with the PP-modified electrode interface. SEM was used to image the biosensor before and after NaOH washing for the PP and NPP samples. As shown in Fig. S2, there were so many nanoparticles loaded on the PP- (Fig. S2 B) and NPP-modified (Fig. S2 E) chip before the NaOH solution washing. After the washing, almost all UiO-66 was washed away from the NPP-modified chip (Fig.S2 F), however, a lot of it remained trapped on the PP-modified chip. All these results demonstrated the success of the washing procedure and the high affinity of the PP samples for UiO-66.

Next, we studied the SPR signal enhancement effect of UiO-66 on the surface of gold chips. As shown in Fig. 2C, after incubation with UiO-66, a prominent high SPR signal was obtained in PP-modified chips (curve i) compared with NPP modified chips (curve ii). This demonstrated the specific affinity of UiO-66 towards the phosphate group, which generated a significant plasma resonance phenomenon with the gold chips. We also compared the ZrO2 and SiO2 results with UiO-66. Although ZrO_2 specifically binds to phosphate residues [24], it does not enhance the SPR effect on the surface of the gold film (As shown in Fig.S3 A). SiO_2 can enhance the SPR effect on the surface of the chip (Fig.S3 B),

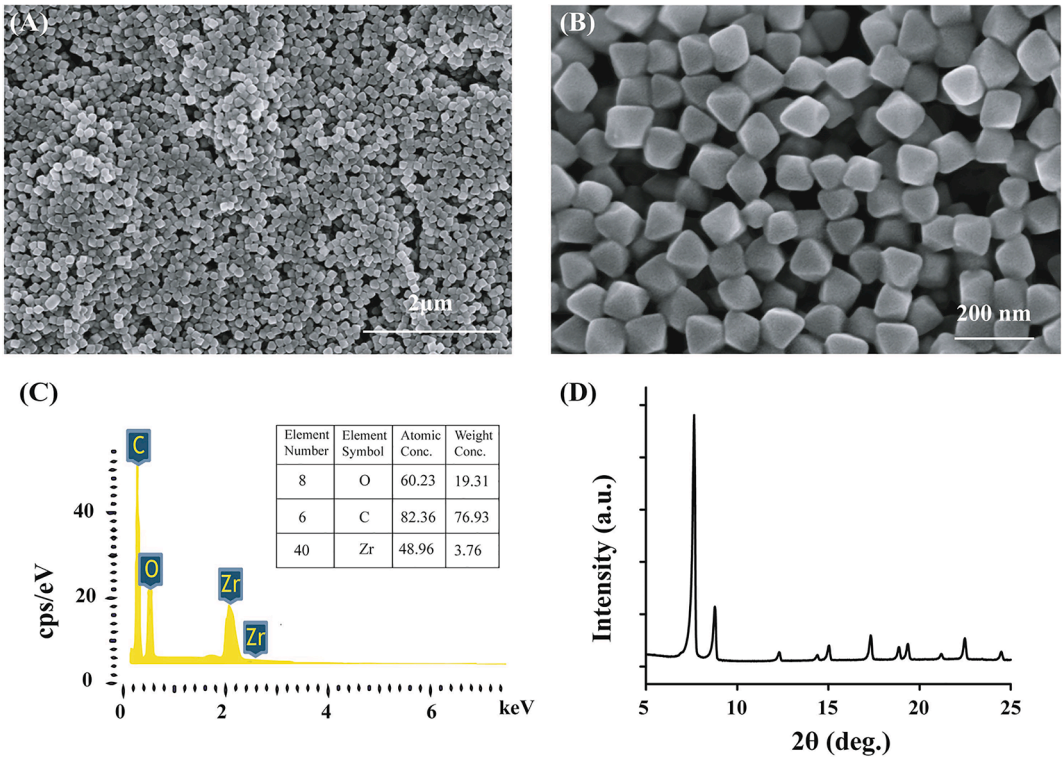

Fig. 1. (A and B) SEM images; (C) EDS, and (D) XRD of synthesized UiO-66 particles.

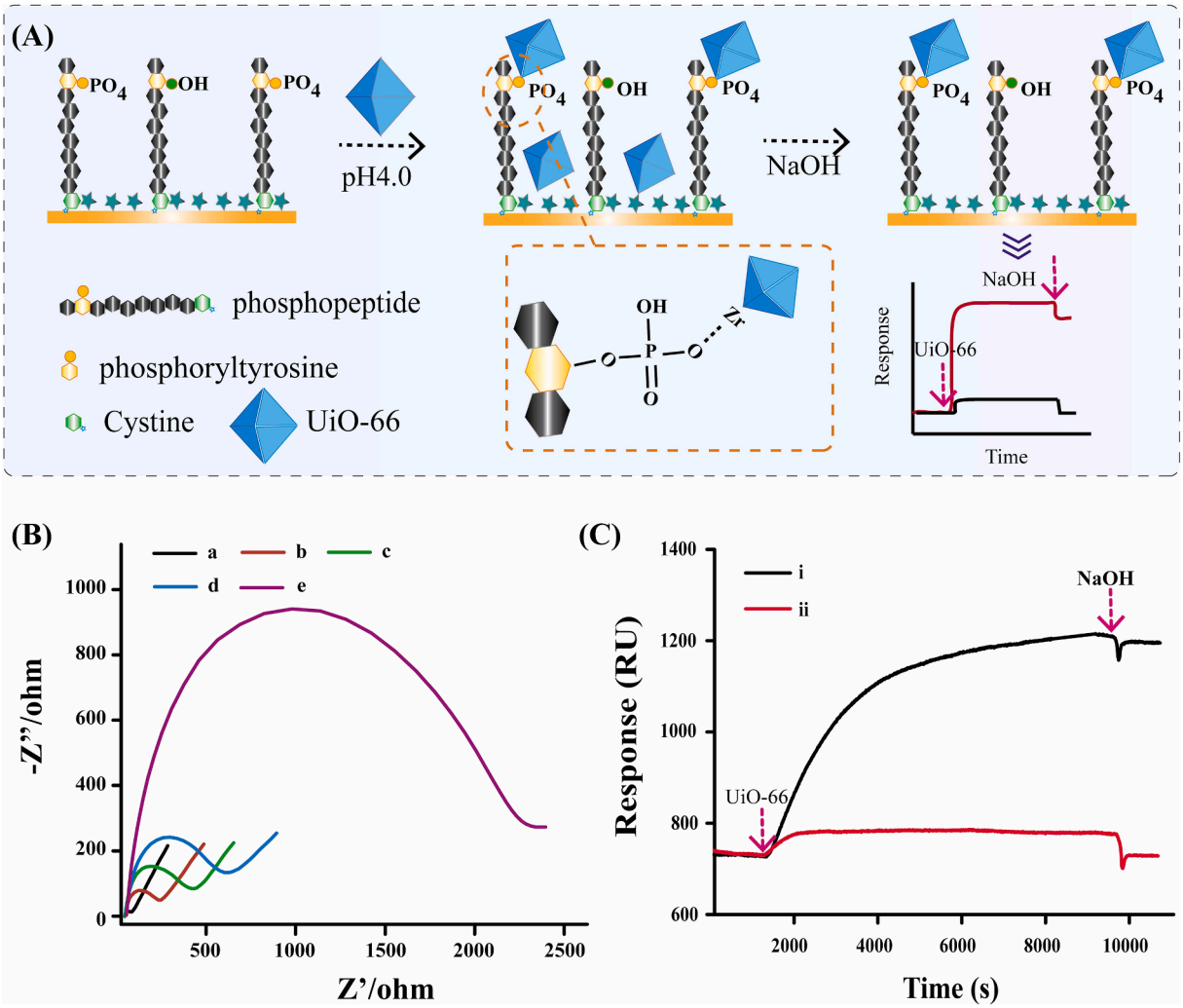

Fig. 2. (A) Illustration of specific binding of UiO-66 to phosphate groups of peptides on the chip surface for SPR signal enhancement; (B) EIS of (a) bare Au electrode, (b) NPP + BSA, (c) PP + BSA, (d) NPP + BSA + UiO-66 and (e) PP + BSA + UiO-66 in 0.1 M KCl containing 5 mM $Fe(CN)_6^{4-/3-}$; (C) SPR sensorgrams of UiO-66 binding with (i) PP and (ii) NPP modified chips.

however, the effect is the same for both PP-modified and NPP-modified chips. This indicates that SiO_2 cannot directly achieve the distinguish of phosphorylated proteins. Therefore, UiO-66 was selected to enhance the SPR effect on the chip and realize the direct detection of phosphorylated proteins. According to the enhancement mechanism of other nanomaterials such as gold, silver, and carbon nanomaterials to SPR, we inferred that UiO-66 can enhance SPR sensing through the following mechanism: (i) the LSPR of nanoparticles coupled with the surface plasmon wave excites the sensing film; (ii) large surface mass loading, and (iii) charge transfer from the nanomaterial surface to the metallic sensing film surface induce a larger evanescent field thereby magnifying the SPR signal [46]. Importantly, the binding between UiO-66 and phosphate group was stable while NaOH wash could fully eliminate the non-specific absorption. This result confirms the high selectivity of the proposed biosensor involving UiO-66 binding to phosphate group via Zr^{4+} [47].

3.4. Influence of pH on the detection specificity

To reduce the influence of peptide chain steric hindrance affecting the sensitivity of the method, the concentration of modified peptide chains on the surface of the gold chip was optimized (Fig. S4). 50 μM peptide chains with the optimal signal-to-noise ratio (S/N) were chosen for the subsequent experiments. To investigate the phosphate sorption of the Zr-based MOFs with different sizes, the UiO-66 with the sizes of 40 ± 10 nm and 300 ± 30 nm were also synthesized by adjusting the volume of acetic acid. As shown in Fig. S5, there were conspicuous SPR responses in Fig. S5 B (120 ± 30 nm) compared with Fig. S5 A (40 ± 10 nm) and Fig. S5 C (300 ± 30 nm). Interestingly, the SPR signal of UiO-66 with 40 ± 10 nm size was completely washed away by the reaction buffer (Fig. S5 A), and the synthesized UiO-66 did not show the typical octahedral structure (the insert of Fig. S5 A). This might affect the identity of UiO-66 to phosphate peptides. Also, a lower SPR response was observed in Fig. S5 C for two reasons: first, there was less binding between UiO-66 and phosphate peptides due to the steric hindrance effect of the large particle size; second, the UiO-66 influence on the surface electric field strength of the gold film was lower. Therefore, Zr-MOF with 120 ± 30 nm size was chosen in this work.

In order to investigate the influence of pH on UiO-66 binding to phosphate groups, 10 mM GTA solution of different pH was used as the UiO-66 binding buffer. As shown in Fig. 3A, an increase in pH gradually decreased the SPR signal of UiO-66 for both PP- and NPP-modified chips. The S/N reached the plateau at pH 4.0–5.0 and then decreased with a further increase in pH. This phenomenon can be attributed to the point of zero charge (PZC; the pH at which the net surface charge is zero), which was about pH 4.7 for UiO-66 (Fig. 3B) [48]. At binding pH lower than PZC, the UiO-66 surface became protonated and positively charged, increasing nonspecific adsorption of UiO-66. While, at pH >

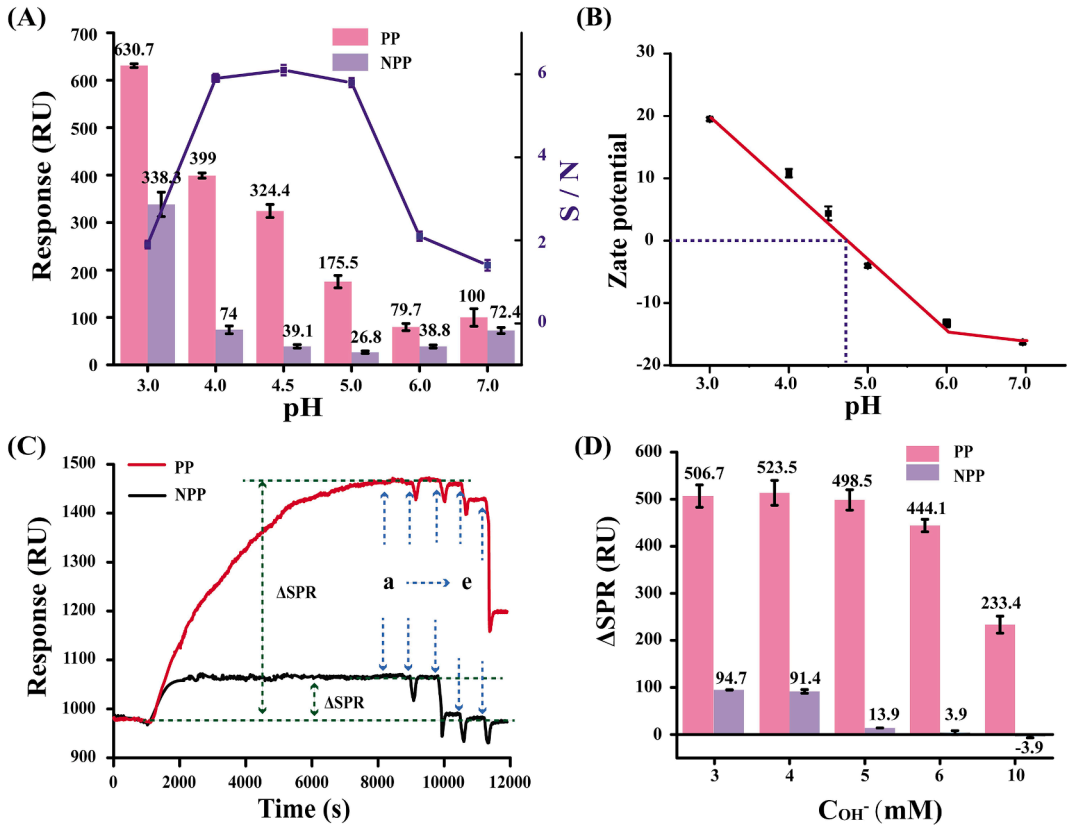

Fig. 3. (A) SPR signal response of UiO-66 binding on peptide-modified chips to different pH binding buffers. (B) UiO-66 surface potential under different pH conditions. (C) The influence of NaOH cleaning solution concentration 3, 4, 5, 6, and 10 mM (from a to e, respectively) on SPR signal. ΔSPR is the SPR signal of UiO-66 after NaOH solution cleaning. (D) The relation of ΔSPR with the concentration of NaOH cleaning solution. Error bars are standard derivations obtained from three independent experiments.

5.0, a higher negative charge was produced on the nanoparticle surface (Fig. 3B) [49]. On the contrary, with an increase in pH, the phosphate species on the phosphorylated peptide progressively change from $H_2PO_4^-$ to HPO_4^{2-} to PO_4^{3-} increasing the negative charge [50,51]. This created a higher repulsive force between the phosphate residues and UiO-66 decreasing S/N. Notably, acidic conditions were well known to change the structure of antibodies and antigens decreasing the binding affinity of immune-complex leading to antigen leaching from the immune-affinity layer. However, several studies suggested that the binding force between antibody and antigen does not change in the investigated pH range of 4.0–12.0, however, the number of interaction events 'counts' could be higher at lower pH (pH $\leq$ 5.0) [52]. Also, pH 2.5 induces an artificial ELISA signal potentially due to IgG rather than other serum proteins [53]. Above all, pH 4.0 was chosen as the optimal condition for UiO-66 binding in the subsequent experiments.

To further eliminate the non-specific adsorption of UiO-66, NaOH solution was used as a cleaning solution and its concentration was optimized. As displayed in Fig. 3C, after binding with UiO-66, the chips were washed with NaOH solutions with incremental concentrations (from a to e). The SPR signal of the NPP-modified chip decreased sharply almost to the initial baseline after washing with 5 mM NaOH solution. Even though the concentration of NaOH continued to increase, the SPR signal held steady (black curve). The SPR signal of the PP group did not show a significant change after washing with $<$ 6 mM NaOH cleaning solutions (red curve). This result indicated that a 5 mM NaOH solution could eliminate the non-specific absorption of UiO-66 without affecting its specific binding. However, when the concentration of NaOH solution increased to 10 mM, the SPR signal of the PP group showed a sharp decline. This indicated that the specific coordination bond of UiO-66 with phosphate species was broken at this NaOH concentration. The biosensor synthesized in this work could not be regenerated. However, after the chip was washed with piranha solution which destroyed the ligands modified on the chip, antibodies and peptides could be re-modified on the chip for the detection of phosphate. This way the chip in this work could be reused about 30 times. The ΔSPR was used to quantify the specific binding of UiO-66 and found that 5 mM NaOH solution was the optimal cleaning solution concentration (Fig. 3D).

3.5. Sensitivity of the biosensor

Under the optimum conditions, the sensitivity of the designed biosensor was examined by preparing different peptide-modified chips with a series coverage of PP ratios. As depicted in Fig. 4A, the SPR signal began to rise after UiO-66 addition and displayed distinct SPR intensities for PP and NPP groups after ~ 90 min. Next, 5 mM NaOH solution was used to wash away the non-specifically adsorbed UiO-66 until the signal became stable. The final signal was recorded as ΔSPR. As shown in Fig. 4, ΔSPR signals gradually increased with the increasing coverage (%) of the phosphorylated peptide showing a linear relationship between the two (from 1% to 100%, Fig. 4B). The linear regression equation is ΔSPR = 4.574 * PP% + 104 with a correlation coefficient of 0.9883. Notably, the limit of detection (LOD) of our SPR biosensor for the coverage of phosphorylated peptides was about 1%. Such high sensitivity can be attributed to the significant SPR enhancement of UiO-66 and its highly specific pH-adjusted binding to phosphate residues. Table 1 summarizes different detection methods of phosphorylated peptides or proteins. The sensitivity of our method is almost comparable to those methods. Compared with the traditional detection methods (Table S1) [54,55], this method is more economical (about 4.3$/test), and the detection time is shortened to 90 min. In addition, the method

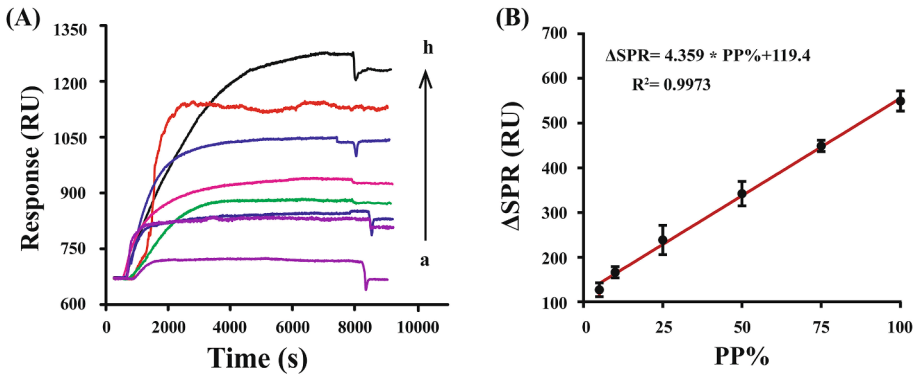

Fig. 4. (A) SPR sensorgrams of 5, 10, 17, 25, 50, 75, and 100% phosphorylated peptides (from a to h, respectively). (B) ΔSPR signal response shows a linear relationship with the increasing coverage of phosphorylated peptides on the chip (1, 5, 10, 25, 50, 75, and 100%). Error bars represent the standard deviations of three different measurements for each concentration.

Table 1
Comparison of sensitivity between different phosphorylation detection assays.

Sensor Structure	Assay type	Target	linear dynamic range	LOD	Ref.
Zn^{2+}-PO_4^{3-}	Fluorescence/FLIM	p-Tau	1.0–5.0 μM	85.15 nM	[56]
Ti^{4+}-PO_4^{3-}	Electrochemical/ Ti^{4+}@TiP/SWV	p-Aβ40	1 fM-100 pM	0.45 fM	[57]
Zr^{4+}-PO_4^{3-}	ratiometric Fluorescence/ UiO-66(Fe/Zr)–NH2	phosphate ion	0.2–266.7 μM	85 nM	[58]
Antigen-antibody	ELISA	p-αS	0.25 ~ 2 ng/mL	50 pg/mL	[59]
Tb^{3+}-PO_4^{3-}	Luminescentsensor/Tb^{3+}	di-phosphorylated peptide	500–0.244 μM	0.2 μM	[60]
Immunoaffinity	Fluorescence	pTyr proteins	–	8 μg	[61]
Zr^{4+}-PO_4^{3-}	UiO-66/SPR	Phosphorylated peptides/protein	0%-100% PP in peptides complex	1%/0.5 μM	This work

FLIM: Fluorescence lifetime imaging microscopy; p-Tau: Hyperphosphorylated Tau; SWV: Square wave voltammetry; p-Aβ40: Phosphorylated Amyloid-β40; SPR: Surface Plasmon Resonance; ELISA: enzyme-linked immunosorbent assay; FRET: Fluorescent Resonance Energy Transfer; QD: Quantum Dots.

does not involve the pre-enrichment and denaturation of phosphorylated proteins into peptide chains, which greatly simplifies the operation process.

3.6. *Distinguishing phosphoprotein from complex samples*

Phosphorylated Akt (p-Akt), the most critical signal molecule in the phosphatidylinositol-4,5-bisphosphate 3-kinase (PI3K)-Akt signaling pathway, has been linked to human breast cancer [62,63]. To estimate the feasibility of the developed SPR biosensor for the detection of phosphoproteins in cells extracts, p-Akt was selected as a model target. Anti-p-Akt (Fig. 5A) and anti-total Akt (Fig. 5B) antibody-modified chips were used to capture corresponding proteins from MDA-MB-231 breast cancer cells extracts. UiO-66 was utilized to distinguish phosphorylated protein and obtain a significantly enhanced SPR signal.

As shown in Fig. 5A, SPR signals of proteins were faint for both p-Akt containing and control extracts. However, a distinctive curve was observed when UiO-66 was injected to bind with p-Akt, while other control groups did not show an obvious SPR signal. Especially, the addition of LY294002 to inhibit the protein phosphorylation of MDA-MB-231 significantly decreased the SPR biosensor signal for p-Akt. This is consistent with the Western blotting results (Fig. 5D a). Also, p-Akt could be specifically distinguished from total Akt after binding to anti-total Akt antibodies (Fig. 5B). However, the SPR signal was lower than that of the anti-p-Akt antibody-modified chip. These results demonstrated that the designed biosensor could capture and identify target phosphorylated protein in a cell extract without requiring separation or purification step.

The N-methyl D-aspartate (NMDA) receptor subtype 2B (NR2B) is considered an important tyrosine-phosphorylated protein in the brain. Its phosphorylation is closely related to increasing Ca^{2+} entry through the receptor in both central sensitization and NMDA-dependent synaptic plasticity [64,65]. A previous study in the chronic migraine rat model found that phosphorylated NR2B (p-NR2B) was highly expressed and might decrease pain thresholds [66]. To further examine the feasibility of the proposed biosensor, the phosphorylation level of NR2B protein in TNC tissues of CM rats was detected with anti-p-NR2B antibody-modified chip. As shown in Fig. 5C, the CM rat group showed a distinct SPR response compared with the normal rat group and other controls, indicating the high expression of phosphorylated NR2B protein in the CM rat. The result is also consistent with Western blotting results (Fig. 5D (b)). Therefore, this method was found feasible for monitoring the level of phosphorylated protein in tissue samples. To sum up, the proposed strategy can directly assess the phosphorylation level of target proteins in cell and tissue extracts by integrating all the operations such as target capture, specific recognition of phosphate residues, and signal enhancement in a single workflow.

4. Conclusion

In summary, an SPR sensor was developed to detect the phosphorylation level of a target protein using the antibody-modified gold chips. This sensor showed high sensitivity and specificity for phosphopeptides and phosphoproteins due to its specificity for phosphate residues and the SPR signal enhancement effect of UiO-66. Furthermore, optimizing the pH conditions and the concentration of NaOH washing solution improved reaction specificity by adjusting the surface charge of the nanoparticles. The designed SPR biosensor was successfully applied to quantitatively analyze the phosphorylated proteins in complex samples validating the excellent accuracy and practicability of the method. The proposed strategy has great potential for multi-component analysis of phosphorylated protein without further separation and purification, which can significantly promote biological and clinical research.

Declaration of Competing Interest

The authors declare that they have no known competing financial interests or personal relationships that could have appeared to influence

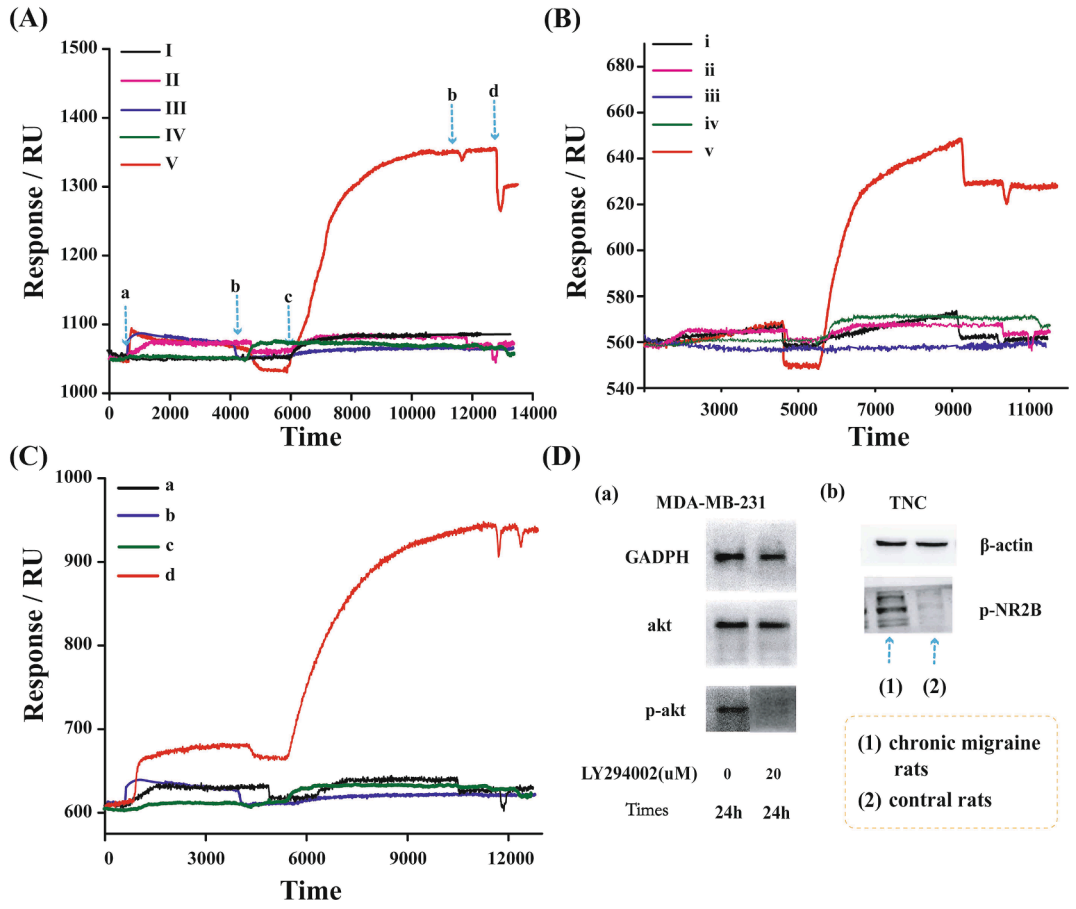

Fig. 5. (A) SPR sensorgrams of captured p-Akt from protein extract using the anti-p-Akt antibody-modified chip and UiO-66 binding (V); GTA buffer (I); protein extract on naked chip (II); Akt (III), protein extract of LY294002-inhibited cells as controls (IV). Steps: a, protein extract incubation; b, GTA buffer washing; c, UiO-66 incubation; d, NaOH solution washing. (B) SPR sensorgrams of captured total Akt from protein extract using the anti-total Akt antibody-modified chip and UiO-66 binding (v); GTA buffer (i); protein extract on naked chip (ii); Akt (iii); protein extract of LY294002-inhibited cells as controls (iv). (C) SPR sensorgrams of captured p-NR2B from TNC tissues of CM rats using the anti-p-NR2B antibody-modified chip and UiO-66 binding (d); GTA buffer (a); non-phosphorylated NR2B (b); protein extract of TNC from normal rats as controls (c). (D) Western blotting results of p-Akt in protein extract from cell lines (a) and p-NR2B in protein extract from TNC tissues of rats.

the work reported in this paper.

Acknowledgements

This work was funded by the National Natural Science Foundation of China (81572080 and 81873972), Hainan Province Clinical Medical Center, Science and Technology Plan of Hainan Province (Clinical Research Center), the Natural Science Foundation Project of Chongqing (cstc2015shmszx120086), and the Chongqing Science Fund for Distinguished Young Scholars (cstc2019jcyjjqX0028). The Foundation for Innovative Research Groups of Chongqing Higher Education Institutions (CXQT20013). The authors would like to thank all the reviewers who participated in the review and MJEditor (www.mjeditor.com) for its linguistic assistance during the preparation of this article.

Appendix A. Supplementary data

Supplementary data to this article can be found online at https://doi.org/10.1016/j.cej.2022.137000.

References

[1] S.Y. Hwang, J.K. Choi, Sensitive phosphoprotein detection in SDS-PAGE via Anthracene Chrome Red A stain, 38(24) (2017) 3079-3085. https://doi.org/10.1002/elps.201700243.

[2] T. Ma, M.A. Trinh, A.J. Wexler, C. Bourbon, E. Gatti, P. Pierre, D.R. Cavener, E. Klann, Suppression of eIF2α kinases alleviates Alzheimer's disease-related plasticity and memory deficits, Nat. Neurosci. 16 (9) (2013) 1299–1305, https://doi.org/10.1038/nn.3486.

[3] B. Ruprecht, S. Lemeer, Proteomic analysis of phosphorylation in cancer, Expert Review Proteomics 11 (3) (2014) 259–267, https://doi.org/10.1586/14789450.2014.901156.

[4] A. Hagner-McWhirter, Y. Laurin, A. Larsson, E.J. Bjerneld, O. Ronn, Cy5 total protein normalization in Western blot analysis, Anal. Biochem. 486 (2015) 54–61, https://doi.org/10.1016/j.ab.2015.06.017.

[5] E. Kinoshita, E. Kinoshita-Kikuta, T. Koike, Separation and detection of large phosphoproteins using Phos-tag SDS-PAGE, Nat. Protoc. 4 (10) (2009) 1513–1521, https://doi.org/10.1038/nprot.2009.154.

[6] E. Maes, K. Tirez, G. Baggerman, D. Valkenborg, L. Schoofs, J.R. Encinar, I. Mertens, The use of elemental mass spectrometry in phosphoproteomic applications, Mass Spectrom. Rev. 35 (3) (2016) 350–360, https://doi.org/10.1002/mas.21440.

[7] H. Marx, S. Lemeer, J.E. Schliep, L. Matheron, S. Mohammed, J. Cox, M. Mann, A. J. Heck, B. Kuster, A large synthetic peptide and phosphopeptide reference library for mass spectrometry-based proteomics, Nat. Biotechnol. 31 (6) (2013) 557–564, https://doi.org/10.1038/nbt.2585.

[8] D. Hussain, S.G. Musharraf, M. Najam-ul-Haq, Development of diamond-lanthanide metal oxide affinity composites for the selective capture of endogenous serum phosphopeptides, Anal. Bioanal. Chem. 408 (6) (2016) 1633–1641, https://doi.org/10.1007/s00216-015-9272-3.

[9] L. Zhu, K. Wang, J. Cui, H. Liu, X. Bu, H. Ma, W. Wang, H. Gong, C. Lausted, L. Hood, G. Yang, Z. Hu, Label-free quantitative detection of tumor-derived exosomes through surface plasmon resonance imaging, Anal. Chem. 86 (17) (2014) 8857–8864, https://doi.org/10.1021/ac5023056.

[10] M. Najam-ul-Haq, F. Jabeen, D. Hussain, A. Saeed, S.G. Musharraf, C.W. Huck, G. K. Bonn, Versatile nanocomposites in phosphoproteomics: a review, Anal. Chim. Acta 747 (2012) 7–18, https://doi.org/10.1016/j.aca.2012.08.004.

[11] D. Xu, M. Gao, C. Deng, X. Zhang, Synthesis of bifunctional TiO2@SiO2-B(OH)2@Fe3O4@TiO2 sandwich-like nanosheets for sequential selective enrichment of phosphopeptides and glycopeptides for mass spectrometric analysis, Anal. Bioanal. Chem. 408 (20) (2016) 5489–5497, https://doi.org/10.1007/s00216-016-9647-0.
[12] X. Zhang, Q. Lu, C. Chen, X. Li, G. Qing, T. Sun, X. Liang, Smart polymers driven by multiple and tunable hydrogen bonds for intact phosphoprotein enrichment, Sci. Technol. Adv. Mater. 20 (1) (2019) 858–869, https://doi.org/10.1080/14686996.2019.1643259.
[13] J. Peng, H. Zhang, X. Li, S. Liu, X. Zhao, J. Wu, X. Kang, H. Qin, Z. Pan, R. Wu, Dual-metal centered zirconium–organic framework: A metal-affinity probe for highly specific interaction with phosphopeptides, Dual-Metal Centered Zirconium-Organic Framework: A Metal-Affinity Probe for Highly Specific Interaction with Phosphopeptides 8 (51) (2016) 35012–35020.
[14] A. Saeed, D. Hussain, S. Saleem, S. Mehdi, R. Javeed, F. Jabeen, M. Najam-Ul-Haq, Metal-organic framework-based affinity materials in proteomics, Anal. Bioanal. Chem. 411 (9) (2019) 1745–1759, https://doi.org/10.1007/s00216-019-01610-x.
[15] M.-M. Wang, S. Chen, Y.-L. Yu, J.-H. Wang, Novel Ti 4+ -chelated polyoxometalate/polydopamine composite microspheres for highly selective isolation and enrichment of phosphoproteins, ACS Appl. Mater. Interfaces 11 (41) (2019) 37471–37478.
[16] X. Zhu, J. Gu, J. Yang, Z. Wang, Y. Li, L. Zhao, W. Zhao, J. Shi, Zr-based metal-organic frameworks for specific and size-selective enrichment of phosphopeptides with simultaneous exclusion of proteins, J. Mater. Chem. B 3 (20) (2015) 4242–4248, https://doi.org/10.1039/c5tb00113g.
[17] G. Kumar, A Simple Method for Detecting Phosphorylation of Proteins by Using Zn (2+)-Phos-Tag SDS-PAGE at Neutral pH, Methods in molecular biology (Clifton, N. J.) 1853 (2018) 223-229.
[18] M. Örd, M. Loog, Detection of Multisite Phosphorylation of Intrinsically Disordered Proteins Using Phos-tag SDS-PAGE, Methods in molecular biology (Clifton, N.J.) 2141 (2020) 779-792.
[19] T.T. Chen, J.T. Yi, Y.Y. Zhao, X. Chu, Biomineralized metal-organic framework nanoparticles enable intracellular delivery and endo-lysosomal release of native active, Proteins 140 (31) (2018) 9912–9920, https://doi.org/10.1021/jacs.8b04457.
[20] K. Dong, Z. Wang, Y. Zhang, J. Ren, X. Qu, Metal-organic framework-based nanoplatform for intracellular environment-responsive endo/lysosomal escape and enhanced, Cancer Therapy 10 (38) (2018) 31998–32005.
[21] N. Zhou, F. Su, C. Guo, L. He, Z. Jia, M. Wang, Q. Jia, Z. Zhang, S. Lu, Two-dimensional oriented growth of Zn-MOF-on-Zr-MOF architecture: A highly sensitive and selective platform for detecting cancer markers, Biosens. Bioelectron. 123 (2019) 51–58, https://doi.org/10.1016/j.bios.2018.09.079.
[22] M. Cinier, M. Petit, F. Pecorari, D.R. Talham, B. Bujoli, C. Tellier, Engineering of a phosphorylatable tag for specific protein binding on zirconium phosphonate based microarrays, Journal of biological inorganic chemistry : JBIC : a publication of the Society of Biological, Inorg. Chem. 17 (3) (2012) 399–407, https://doi.org/10.1007/s00775-011-0863-y.
[23] G.-Y. Zhang, C. Cai, S. Cosnier, H.-B. Zeng, X.-J. Zhang, D. Shan, Zirconium–metalloporphyrin frameworks as a three-in-one platform possessing oxygen nanocage, electron media, and bonding site for electrochemiluminescence protein kinase activity assay, Nanoscale 8 (22) (2016) 11649–11657, https://doi.org/10.1039/c6nr01206j.
[24] Y. Gu, D. Xie, Y. Ma, W. Qin, H. Zhang, G. Wang, Y. Zhang, H. Zhao, Size modulation of zirconium-based metal organic frameworks for highly efficient phosphate remediation, ACS Appl. Mater. Interfaces 9 (37) (2017) 32151–32160, https://doi.org/10.1021/acsami.7b10024.
[25] M. Zhao, C. Deng, X. Zhang, The design and synthesis of a hydrophilic core–shell–shell structured magnetic metal–organic framework as a novel immobilized metal ion affinity platform for phosphoproteome research, Chem. Commun. 50 (47) (2014) 6228, https://doi.org/10.1039/c4cc01038h.
[26] B. Luo, M. Yang, P. Jiang, F. Lan, Y. Wu, Multi-affinity sites of magnetic guanidyl-functionalized metal-organic framework nanospheres for efficient enrichment of global phosphopeptides, Nanoscale 10 (18) (2018) 8391–8396, https://doi.org/10.1039/c8nr01914b.
[27] J. Ashley, M. Piekarska, C. Segers, L. Trinh, T. Rodgers, R. Willey, I.E. Tothill, An SPR based sensor for allergens detection, Biosens. Bioelectron. 88 (2017) 109–113, https://doi.org/10.1016/j.bios.2016.07.101.
[28] W. Vandezande, K.P.F. Janssen, F. Delport, R. Ameloot, D.E. De Vos, J. Lammertyn, M.B.J. Roeffaers, Parts per million detection of alcohol vapors via metal organic framework functionalized surface plasmon resonance sensors, Anal. Chem. 89 (8) (2017) 4480–4487, https://doi.org/10.1021/acs.analchem.6b04510.
[29] C. Zhou, H. Zou, C. Sun, D. Ren, J. Chen, Y. Li, Signal amplification strategies for DNA-based surface plasmon resonance biosensors, Biosens. Bioelectron. 117 (2018) 678–689, https://doi.org/10.1016/j.bios.2018.06.062.
[30] Y.U. Kayran, D. Ozkan-Ariksoysal, S.N. Topkaya, B.T. Kaymaz, B.K. Can, Cystic fibrosis mutation detection with SPR biosensor in real samples via multiple surfaces binding method, Comb. Chem. High Throughput Screening 20 (1) (2017) 56–63, https://doi.org/10.2174/1386207320666170103154226.
[31] M.Z. Mousavi, H.Y. Chen, S.H. Wu, S.W. Peng, K.L. Lee, P.K. Wei, J.Y. Cheng, Magnetic nanoparticle-enhanced SPR on gold nanoslits for ultra-sensitive, label-free detection of nucleic acid biomarkers, The Analyst 138 (9) (2013) 2740–2748, https://doi.org/10.1039/c3an36655c.
[32] X. Wei, X. Duan, X. Zhou, J. Wu, H. Xu, X. Min, S. Ding, A highly sensitive SPRi biosensing strategy for simultaneous detection of multiplex miRNAs based on strand displacement amplification and AuNP signal enhancement, The Analyst 143 (13) (2018) 3134–3140, https://doi.org/10.1039/c8an00549d.
[33] B. Douzi, Protein-protein interactions: surface plasmon resonance, methods in molecular biology (Clifton, N.J.) (1615 (2017)) 257–275, https://doi.org/10.1007/978-1-4939-7033-9_21.
[34] A. Olaru, C. Bala, N. Jaffrezic-Renault, H.Y. Aboul-Enein, Surface plasmon resonance (SPR) biosensors in pharmaceutical analysis, Crit. Rev. Anal. Chem. 45 (2) (2015) 97–105, https://doi.org/10.1080/10408347.2014.881250.
[35] S.Y. Yin, G. Song, Y. Yang, Y. Zhao, P. Wang, L.M. Zhu, X. Yin, X.B. Zhang, Persistent regulation of tumor microenvironment via circulating catalysis of MnFe2O4@Metal–organic frameworks for enhanced photodynamic therapy, Adv. Funct. Mater. 29 (25) (2019) 1901417, https://doi.org/10.1002/adfm.201901417.
[36] X. Zhu, J. Gu, Y. Wang, B. Li, Y. Li, W. Zhao, J. Shi, Inherent anchorages in UiO-66 nanoparticles for efficient capture of alendronate and its mediated release, Chem. Commun. (Camb.) 50 (63) (2014) 8779–8782, https://doi.org/10.1039/c4cc02570a.
[37] X. Zhu, B. Li, J. Yang, Y. Li, W. Zhao, J. Shi, J. Gu, Effective adsorption and enhanced removal of organophosphorus pesticides from aqueous solution by Zr-based MOFs of UiO-67, ACS Appl. Mater. Interfaces 7 (1) (2015) 223–231, https://doi.org/10.1021/am5059074.
[38] C. Guo, F. Su, Y. Song, B. Hu, M. Wang, L. He, D. Peng, Z. Zhang, Aptamer-templated silver nanoclusters embedded in zirconium metal-organic framework for bifunctional electrochemical and SPR aptasensors toward carcinoembryonic antigen, ACS Appl. Mater. Interfaces 9 (47) (2017) 41188–41199, https://doi.org/10.1021/acsami.7b14952.
[39] W. Zhang, Y. Wang, J. Guo, Y. Yu, W. Duan, Y. Yang, X. Bai, B. Liu, Optimization of plasmonic metal structures for improving the hydrogen production efficiency of metal-organic frameworks, Nanoscale 13 (24) (2021) 10807–10815, https://doi.org/10.1039/d1nr01197a.
[40] Y. Bai, Y. Dou, L.H. Xie, W. Rutledge, J.R. Li, H.C. Zhou, Zr-based metal-organic frameworks: design, synthesis, structure, and applications, Chem. Soc. Rev. 45 (8) (2016) 2327–2367, https://doi.org/10.1039/c5cs00837a.
[41] Y. Zhou, L.B. Zhu, A.F. Peng, T.F. Wang, X.H. Long, S. Gao, R.P. Zhou, Z.L. Liu, LY294002 inhibits the malignant phenotype of osteosarcoma cells by modulating the phosphatidylinositol 3-kinase/Akt/fatty acid synthase signaling pathway in vitro, Mol. Med. Rep. 11 (2) (2015) 1352–1357, https://doi.org/10.3892/mmr.2014.2787.
[42] Y. Fan, X. Duan, M. Zhao, X. Wei, J. Wu, W. Chen, P. Liu, W. Cheng, Q. Cheng, S. Ding, High-sensitive and multiplex biosensing assay of NSCLC-derived exosomes via different recognition sites based on SPRi array, Biosens. Bioelectron. 154 (2020), 112066, https://doi.org/10.1016/j.bios.2020.112066.
[43] W. Morris, W.E. Briley, E. Auyeung, M.D. Cabezas, C.A. Mirkin, Nucleic acid-metal organic framework (MOF) nanoparticle conjugates, J. Am. Chem. Soc. 136 (20) (2014) 7261–7264, https://doi.org/10.1021/ja503215w.
[44] H. Wu, Y.S. Chua, V. Krungleviciute, M. Tyagi, P. Chen, T. Yildirim, W. Zhou, Unusual and highly tunable missing-linker defects in zirconium metal-organic framework UiO-66 and their important effects on gas adsorption, J. Am. Chem. Soc. 135 (28) (2013) 10525–10532, https://doi.org/10.1021/ja404514r.
[45] S. Wang, C.M. McGuirk, M.B. Ross, S. Wang, P. Chen, H. Xing, Y. Liu, C.A. Mirkin, General and Direct Method for Preparing Oligonucleotide-Functionalized Metal-Organic Framework Nanoparticles, J. Am. Chem. Soc. 139 (29) (2017) 9827–9830, https://doi.org/10.1021/jacs.7b05633.
[46] S. Zeng, D. Baillargeat, H.P. Ho, K.T. Yong, Nanomaterials enhanced surface plasmon resonance for biological and chemical sensing applications, Chem. Soc. Rev. 43 (10) (2014) 3426–3452, https://doi.org/10.1039/c3cs60479a.
[47] C. Fu, H. Zhou, L. Tan, Z. Huang, Q. Wu, X. Ren, J. Ren, X. Meng, Microwave-Activated Mn-Doped Zirconium Metal-Organic Framework Nanocubes for Highly Effective Combination of Microwave Dynamic and Thermal Therapies Against Cancer, ACS Nano 12 (3) (2018) 2201–2210, https://doi.org/10.1021/acsnano.7b08868.
[48] H. Liu, X. Sun, C. Yin, C. Hu, Removal of phosphate by mesoporous ZrO2, J. Hazard. Mater. 151 (2–3) (2008) 616–622, https://doi.org/10.1016/j.jhazmat.2007.06.033.
[49] F. Long, J.-L. Gong, G.-M. Zeng, L. Chen, X.-Y. Wang, J.-H. Deng, Q.-Y. Niu, H.-Y. Zhang, X.-R. Zhang, Removal of phosphate from aqueous solution by magnetic Fe–Zr binary oxide, Chem. Eng. J. 171 (2) (2011) 448–455, https://doi.org/10.1016/j.cej.2011.03.102.
[50] P. Delaney, C. McManamon, J.P. Hanrahan, M.P. Copley, J.D. Holmes, M. A. Morris, Development of chemically engineered porous metal oxides for phosphate removal, J. Hazard. Mater. 185 (1) (2011) 382–391, https://doi.org/10.1016/j.jhazmat.2010.08.128.
[51] M.A. Johir, M. Pradhan, P. Loganathan, J. Kandasamy, S. Vigneswaran, Phosphate adsorption from wastewater using zirconium (IV) hydroxide: Kinetics, thermodynamics and membrane filtration adsorption hybrid system studies, J. Environ. Manage. 167 (2016) 167–174, https://doi.org/10.1016/j.jenvman.2015.11.048.
[52] T.-H. Nguyen, A. Greinacher, Effect of pH and ionic strength on the binding strength of anti-PF4/polyanion antibodies, Eur. Biophys. J. 46 (8) (2017) 795–801, https://doi.org/10.1007/s00249-017-1240-8.
[53] Q. Li, M. Gordon, C. Cao, K.E. Ugen, D. Morgan, Improvement of a low pH antigen-antibody dissociation procedure for ELISA measurement of circulating anti-Aβ antibodies, BMC Neuroscience 8 (1) (2007), https://doi.org/10.1186/1471-2202-8-22.
[54] C. Lenz, Identification of Protein Phosphorylation Sites by Advanced LC-ESI-MS/MS Methods, Methods Mol. Biol. 2019 (1934) 163–178, https://doi.org/10.1007/978-1-4939-9055-9_11.
[55] A. Sasaki, S. Arawaka, H. Sato, T. Kato, Sensitive western blotting for detection of endogenous Ser129-phosphorylated alpha-synuclein in intracellular and

extracellular spaces, Sci. Rep. 5 (2015) 14211, https://doi.org/10.1038/srep14211.
[56] L. Ge, Y. Tian, Fluorescence Lifetime Imaging of p-tau Protein in Single Neuron with a Highly Selective Fluorescent Probe, Anal. Chem. 91 (5) (2019) 3294–3301, https://doi.org/10.1021/acs.analchem.8b03992.
[57] Z. Yin, S. Wang, B. Shen, C. Deng, Q. Tu, Y. Jin, L. Shen, B. Jiao, J. Xiang, Coimmunocapture and Electrochemical Quantitation of Total and Phosphorylated Amyloid-β40 Monomers, Anal. Chem. 91 (5) (2019) 3539–3545, https://doi.org/10.1021/acs.analchem.8b05307.
[58] X. Li, P. Liu, X. Niu, K. Ye, L. Ni, D. Du, J. Pan, Y. Lin, Tri-functional Fe–Zr bi-metal–organic frameworks enable high-performance phosphate ion ratiometric fluorescent detection, Tri-functional Fe-Zr bi-metal-organic frameworks enable high-performance phosphate ion ratiometric fluorescent detection 12 (37) (2020) 19383–19389.
[59] N.K. Majbour, N.N. Vaikath, K.D. van Dijk, M.T. Ardah, S. Varghese, L. B. Vesterager, L.P. Montezinho, S. Poole, B. Safieh-Garabedian, T. Tokuda, C. E. Teunissen, H.W. Berendse, W.D.J. van de Berg, O.M.A. El-Agnaf, Oligomeric and phosphorylated alpha-synuclein as potential CSF biomarkers for Parkinson's disease, Mol. Neurodegener. 11 (1) (2016), https://doi.org/10.1186/s13024-016-0072-9.
[60] E. Duodu, D. Kraskouskaya, J. Campbell, G. Graca-Lima, P.T. Gunning, Selective detection of tyrosine-containing proximally phosphorylated motifs using an antenna-free Tb3+ luminescent sensor, Chem. Commun. 51 (30) (2015) 6675–6677, https://doi.org/10.1039/c5cc00679a.
[61] S. Bergström Lind, Å. Hagner-McWhirter, L. Elfineh, M. Molin, A. Jorsback, J. Öhman, U. Pettersson, Detection of tyrosine phosphorylated proteins by combination of immunoaffinity enrichment, two-dimensional difference gel electrophoresis and fluorescent Western blotting, Biochem. Biophys. Res. Commun. 401 (4) (2010) 581–585.
[62] X. Zhang, Y. Zhao, C. Wang, H. Ju, W. Liu, X. Zhang, S. Miao, L. Wang, Q. Sun, W. Song, Rhomboid domain-containing protein 1 promotes breast cancer progression by regulating the p-Akt and CDK2 levels, Cell Communication and Signaling 16 (1) (2018), https://doi.org/10.1186/s12964-018-0267-5.
[63] K. Wang, F. Cao, W. Fang, Y. Hu, Y. Chen, H. Ding, G. Yu, Activation of SNAT1/SLC38A1 in human breast cancer: correlation with p-Akt overexpression, BMC cancer 13 (2013) 343, https://doi.org/10.1186/1471-2407-13-343.
[64] S. Li, J. Cao, X. Yang, Z.W. Suo, L. Shi, Y.N. Liu, H.B. Yang, X.D. Hu, NR2B phosphorylation at tyrosine 1472 in spinal dorsal horn contributed to N-methyl-D-aspartate-induced pain hypersensitivity in mice, J. Neurosci. Res. 89 (11) (2011) 1869–1876, https://doi.org/10.1002/jnr.22719.
[65] X.X. Qu, J. Cai, M.J. Li, Y.N. Chi, F.F. Liao, F.Y. Liu, Y. Wan, J.S. Han, G.G. Xing, Role of the spinal cord NR2B-containing NMDA receptors in the development of neuropathic pain, Exp. Neurol. 215 (2) (2009) 298–307, https://doi.org/10.1016/j.expneurol.2008.10.018.
[66] X.-Y. Wang, H.-R. Zhou, S. Wang, C.-Y. Liu, G.-C. Qin, Q.-Q. Fu, J.-Y. Zhou, L.-X. Chen, NR2B-Tyr phosphorylation regulates synaptic plasticity in central sensitization in a chronic migraine rat model, The Journal of Headache and Pain 19 (1) (2018), https://doi.org/10.1186/s10194-018-0935-2.